J Mater Sci (2007) 42:3977–3984
DOI 10.1007/s10853-006-1404-x

Investigations on surface composition and microstructure of sintered barium titanate

Sanjiv Kumar · V. S. Raju · T. R. N. Kutty

Received: 4 May 2005 / Accepted: 22 February 2006 / Published online: 31 January 2007

Abstract The paper describes studies on surface atomic composition, microstructure and microarea elemental distribution in sintered undoped as well as donor or acceptor doped polycrystalline barium titanate ceramics. The specimens examined are derived from barium titanate powders synthesized by two different wet chemical procedures namely oxalate precursor route and gel-to-crystallite conversion. The compositional analysis is carried out by backscattering spectrometry (BS) involving 3.05 MeV $^{16}O(\alpha,\alpha)^{16}O$ resonant scattering while investigations on microstructure and microarea elemental distribution are performed using scanning electron microscopy (SEM) and energy dispersive X-ray spectroscopy (EDS), respectively. The specimens prepared by either method are monophasic; however, their surface atomic composition, microstructural features as well as electrical characteristics are significantly different. The specimens obtained by oxalate precursor route generally have Ti rich surfaces and exhibit coarse to fine grained microstructure depending on the nature and extent of doping. The Mn-doped specimens exhibit appreciable O deficiency. The specimens prepared by gel to crystallite conversion, in contrast, usually have Ba enriched surfaces and exhibit fine-grained microstructure. EDS measurements show the segregation of acceptors such as Mn, Cu and Zn in the grain boundaries of oxalate precursor derived ceramics. Further, the relative atomic ratio of Ti to Ba at the sites of segregations is higher compared to other locations.

S. Kumar (✉) · V. S. Raju
National Centre for Compositional Characterization of Materials, Bhabha Atomic Research Centre, ECIL Post, Hyderabad 500062, India
e-mail: sanjiv@cccmindia.org

T. R. N. Kutty
Materials Research Centre, Indian Institute of Science, Bangalore 560012, India

Introduction

Barium titanate has been extensively studied due to its interesting electrical properties such as ferroelectricity, high dielectric constant, piezoelectricity and pyroelectricity [1–4]. Barium titanate is an insulator, however, it acquires semiconducting properties and exhibits positive temperature coefficient resistor (PTCR) characteristics on doping with pentavalent or trivalent cations in small concentrations (≤0.5 at.%). Doping with aliovalent impurities has been effectively used to tailor the electrical properties of $BaTiO_3$ for specific applications [5]. Doping and the subsequent high temperature sintering introduce defects of different kinds in the material. These processes are also accompanied by microstructural changes and alterations in the surface characteristics. The defect chemistry and the microstructural evolution in barium titanate have been subjects of several studies.

There has been an increasing interest in recent years in the surface characterisation of perovskite titanates. Most of the active devices involve the fabrication of thin films and multilayers wherein the understanding of the composition in the surface and near surface regions is important. Previously the

authors have studied the surface chemical states of barium titanate having different electrical properties that result on doping with Sb_2O_5 [6]. However only a few investigations have been made on the compositional analysis in the surface and near surface regions of the ceramic. For example, Auger electron microscopy (AES) and secondary ionization mass spectrometry (SIMS) were used to study the atomic ratio of Ba to Ti at surfaces and interfaces in differently doped barium titanate specimens [7, 8]. It is to be noted that energy dispersive X-ray spectroscopy (EDS), one of the most widely used surface analytical techniques, has found limited application in the analysis of barium titanate in view of severe interference between Ti-K and Ba-L X-rays.

In this study the surface composition of undoped as well as donor or acceptor doped discs of barium titanate, sintered at temperatures >1,350 °C, has been investigated by 3.05 MeV $^{16}O(\alpha,\alpha)^{16}O$ resonant scattering, a backscattering spectrometry (BS) technique. The discs examined are prepared using barium titanate powder synthesized by two different wet chemical procedures namely oxalate precursor route and gel-to-crystallite conversion. The resonant scattering technique is employed to facilitate the determination of oxygen in addition to Ba and Ti, which is difficult by the conventional Rutherford backscattering spectrometry (RBS) in view of the fact that barium titanate is rather a high Z matrix. To the best of our knowledge similar studies have not been performed earlier though this technique has been used in the analysis of various other materials including high temperature superconductors [9].

In addition, we have also studied the microstructure and the segregation of acceptors or donors in the grain boundaries of the barium titanate ceramics. The spatial distributions of donor or acceptor type impurities as well as those of lattice constituents are important in polycrystalline ceramics used in such devices as PTC resistors, grain boundary layer capacitors and varistors. An attempt has been made to correlate the surface composition of the specimens with their microstructural and electrical characteristics.

Experimental

Specimen preparation

Sintered discs of barium titanate prepared by the oxalate precursor method are referred to as discs-A while those prepared by gel-to-crystallite method as discs-B in the succeeding sections. The first method involved high temperature decomposition of barium titanyl oxalate and the second, refluxing of titania gel with barium hydroxide at 110 °C. These methods are described in detail in references [10, 11]. Barium titanate powders prepared by both the methods were doped with 0.3, 0.5 and 0.75 at.% Sb^{5+}, a donor. Further, the powders prepared by oxalate precursor method were also doped with acceptors such as Mn^{2+}, Cu^{2+} and Zn^{2+} in concentration range of 0.25–1.0 at.%. The doping was achieved through the solid-state reaction with the oxides or sulphates of the corresponding elements. The compound required to achieve a specific level of doping was mixed with barium titanate powder homogeneously in an agate mortar, with additions of distilled alcohol. This mixture was further calcined at 1,050 °C in air in clean platinum crucibles for 4 h for interdiffusion to take place. The pellets were made by mixing the relevant powders with polyvinyl alcohol, a binder and compacting in a hydraulic press. These pellets, placed on platinum supports in an alumina boat, were subsequently sintered at 1,380 °C in air for 3 h. The ceramic samples were processed with the same heating and cooling rate of 2 °C/min.

Backscattering spectroscopy measurements

The BS measurements were carried out using 3 MV Tandetron at NCCCM, Hyderabad. The α-particle beam of requisite energy (2.4–3.25 MeV) impinged on the targets at normal incidence in a typical scattering chamber. An electron suppressor with –900 V was placed in front of the samples. The particles scattered at 170° were measured with a surface barrier detector and the data acquired on a PC-based multichannel analyser. The vacuum in the scattering chamber, pumped by a turbomolecular pump, was about 2×10^{-6} torr.

SEM and XRD measurements

The microstructure of the samples was studied by SEM (Philips XL30) while the segregation by the attached EDS system using 20–30 keV electron beam. The intercept method was used to calculate the grain sizes of the crystallites from the SEM micrographs. The phases were identified by X-ray diffraction (XRD) (Scintag 2000, Cu-K_α). The dielectric constants were measured by a Hewlett-Packard precision LCR meter, HP 4284, while the samples were maintained in variable temperature chamber.

Methodological considerations for compositional analysis

Alpha particle RBS can provide the relative atomic ratio of Ba to Ti in the specimens. However it is not suitable for the determination of oxygen due to Z^2 dependence of the Rutherford backscattering cross-section (σ_R) [12]. On the other hand, $^{16}O(\alpha,\alpha)^{16}O$ scattering displays a sharp (FWHM = 11 keV), isolated and strong resonance at 3.05 MeV. The resonant scattering cross section (σ_r) is about 22 times higher than the corresponding σ_R [13]. Therefore this resonance has better sensitivity for oxygen and is also suitable for its depth profiling. The resonant scattering occurs at the surface when the target is bombarded with 3.05 MeV α-particles. It occurs at deeper layers in the target at higher incident energies. Therefore depth profiling of oxygen is accomplished by increasing the incident beam energy beyond 3.05 MeV in steps. The atomic composition of the specimens was determined by comparing the experimental spectra with the simulated spectra obtained by SIMNRA [14]. It is to be noted that (a) the resonant scattering has similar kinematics as that of RBS and (b) the scattering cross sections for Ba and Ti remain Rutherford in the beam energy region presently used.

Results and discussion

The XRD results suggested that the samples did not contain any secondary phase. Barium titanate was present predominantly in tetragonal phase with cubic being the minor phase in all samples except 1.0 at.% Mn doped specimen, in which hexagonal phase is predominant. The undoped barium titanate discs prepared by both methods were pale yellow in colour and insulating. Discs-A doped with 0.3–0.5 at.% Sb were dark blue in colour. These were semiconducting and exhibited PTCR characteristics whereas those doped with >0.5 at.% Sb were grey and dielectric [6]. On the other hand discs-B doped with Sb were grey and dielectric, irrespective of the extent of doping. The dielectric constant vs. temperature plots for 0.75 at.% Sb doped disc-A and 0.3 at.% Sb doped disc-B are shown in Fig. 1a, b, respectively for illustration.

Figure 2 shows typical RBS spectrum of barium titanate obtained using 2.4 MeV α-particles as well as backscattering spectra involving $^{16}O(\alpha,\alpha)^{16}O$ resonant scattering recorded using 3.075 MeV α-particles. The smooth curves shown in the plots are simulated spectra. The signals of Ba, Ti and O in the spectra are indicated. The O signal, seen barely in the 2.4 MeV

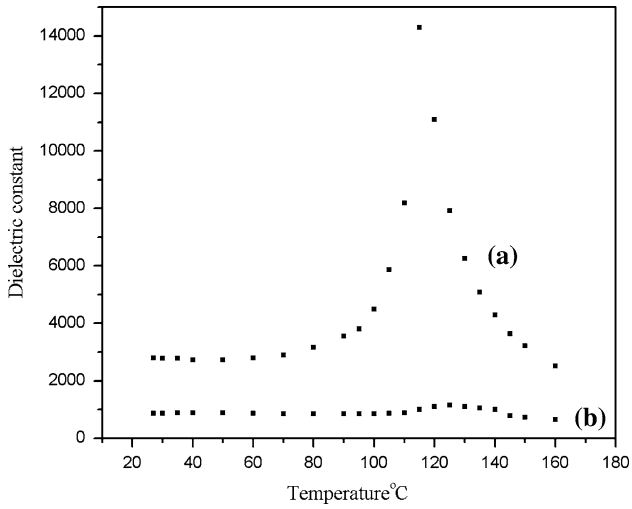

Fig. 1 Dielectric constant vs. temperature plot for (**a**) 0.75 at.% Sb doped barium titanate prepared by oxalate precursor method and (**b**) 0.3 at.% Sb doped barium titanate prepared by gel to crystallite method

α-RBS spectrum exists as a conspicuous peak in a 3.075 MeV α-BS spectrum due to resonant scattering. The compositions of the specimens relative to Ba are listed in Table 1. Measurements performed at different beam energies, for example 3.075 and 3.115 MeV, to depth profile O produced identical compositions. These are accurate to better than ±7% for oxygen and ±3% for the metal constituents.

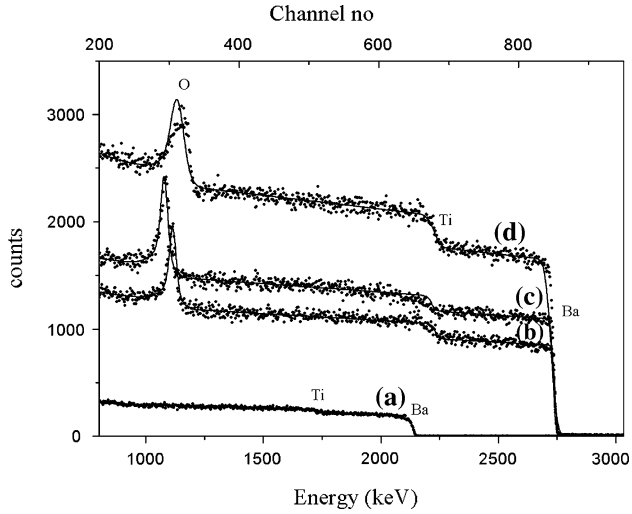

Fig. 2 (**a**) 2.4 MeV α-RBS spectrum from barium titanate and 3.075 MeV α-BS spectra involving $^{16}O(\alpha,\alpha)^{16}O$ resonant scattering from (**b**) undoped and (**d**) and 1.0 at.% Mn doped barium titanate prepared by oxalate precursor method, and (**c**) 0.3 at.% Sb doped barium titanate prepared by gel-to-crystallite conversion. Solid lines are simulated spectra

Table 1 Atomic composition of differently processed barium titanate discs determined by 3.05 MeV $^{16}O(\alpha,\alpha)^{16}O$ resonant scattering

Specimen	Atomic composition
Undoped (oxalate precursor)	Ba $Ti_{1.04}$ $O_{2.7}$
0.3 at.% Sb doped (oxalate precursor)	Ba $Ti_{1.02}$ $O_{3.0}$
0.5 at.% Sb doped (oxalate precursor)	Ba $Ti_{1.02}$ $O_{2.9}$
0.75 at.% Sb doped (oxalate precursor)	Ba $Ti_{1.02}$ $O_{2.9}$
0.5 at.% Cu doped (oxalate precursor)	Ba $Ti_{1.0}$ $O_{2.9}$
0.25 at.% Mn doped (oxalate precursor)	Ba $Ti_{1.09}$ $O_{2.6}$
1.0 at.% Mn doped (oxalate precursor)	Ba $Ti_{1.13}$ $O_{2.3}$
1.0 at.% Mn doped (oxalate precursor)*	Ba $Ti_{1.1}$ $O_{2.4}$
Undoped (gel to crystallite)	Ba $Ti_{0.8}$ $O_{2.7}$
0.3 at.% Sb doped (gel to crystallite)	Ba $Ti_{1.04}$ $O_{3.0}$
0.3 at.% Sb doped (gel to crystallite)*	Ba $Ti_{1.0}$ $O_{2.8}$

* Sliced specimens; other measurements were performed on as sintered specimens

It can be seen that the Mn-doped discs-A are enriched with Ti as compared to the stoichiometry of barium titanate (Ba:Ti::1:1). The enrichment of Ti in other discs-A is marginal considering the error associated with the measurement of the metals. The Table 1, in fact, represents the average cationic ratio over a depth of about 2 μm. However a careful spectral analysis indicates that in undoped and donor doped specimens, the content of Ti exceeds that of Ba by about 10% in about 1,000 Å top layers. This observation is supported by our earlier X-ray photoelectron spectroscopy (XPS) studies on these samples [6]. XPS is a surface analytical technique having a probing depth of about 50 Å. The cationic ratio (N_{Ti}/N_{Ba}) estimated from the peak intensities of Ba($3d_{5/2}$) and Ti($2p_{3/2}$) electrons by taking their respective sensitivity factors into consideration, for example, are 1.16, 1.21 and 1.16 for undoped, 0.5 and 0.75 at.% Sb doped discs-A, respectively. On the other hand, the Table 1 indicates that surfaces of undoped disc-B are enriched with Ba while doping with Sb leads to an increase in Ti content. Interestingly, the cationic ratio (N_{Ti}/N_{Ba}) estimated by XPS for undoped and 0.3 at.% doped discs-B are 0.5 and 0.8, respectively. As XPS and BS have significantly different surface sensitivity, the atomic compositions estimated by the two techniques are indicative of a systematic variation in N_{Ti}/N_{Ba} ratio with depth. It can be surmised by comparing the two sets of data that the specimens tend to acquire stoichiometric cationic ratio at greater depths. These results are in sharp contrast to earlier studies by Desu and Payne [8]. They reported, based on AES analysis, enrichment of surfaces of acceptor doped barium titanate specimens with Ba and those of donor doped specimens with Ti. In some cases the content of Ba on surfaces was found to be as high as about five times the stoichiometry. It is to be noted that these studies were performed on discs prepared by oxalate precursor method. Our observations are consistent with the facts that Ba-titanyl oxalate is formed in strong acid medium and hence tends to Ba deficient whereas the gel to crystallite conversion is carried out in alkaline medium and therefore it tends to be Ba-rich. However, the surface enrichment in sintered specimens depends on a number of other factors such as vacancy formation energy, ion and vacancy mobilities in a complicated way and therefore models formulated to explain such processes are often contradictory.

The content of O in both undoped discs-A and B is less while in donor and Cu doped specimens it is close to the stiochiometry values. Its value depends on two processes namely, (a) loss of oxygen by way of thermodynamic stabilization of O vacancies during sintering and (b) uptake of O from the surroundings during the post sinter annealing at intermediate (850–950 °C) temperatures. However the Mn doped ceramics, in particular 1 at.% doped, exhibit high O deficiency. This result is consistent with the hexagonal structure of the 1.0 at.% doped barium titanate as significantly high density of O vacancies is necessary to enable the microscopic step of transformation from the tetragonal to hexagonal stacking of Ba–O layers. Mn occupying the Ti-sites act as acceptors by way of oxygen vacancy compensation since holes in wide band gap materials such as barium titanate are non-prevalent. The presence of defect complex such as (Mn^{2+}–V_o) was confirmed by the electron paramagnetic resonance spectra [15]. Oxygen deficiency of nearly similar magnitude was reported in an X-ray scattering study on iron doped hexagonal phase of barium titanate [16]. In a recent study involving high resolution imaging by transmission electron microscopy Jia and Urban have reported about 33% O vacancy along the twin boundaries in barium titanate thin films [17].

Measurements on the as-sintered as well as sliced surfaces of two other Mn doped (1.0 at.%) specimens, performed in view of rather interesting results yielded identical composition. It is also worth mentioning that the peak width of O signal in the backscattered spectra for these Mn doped specimens is considerably larger than those of the other specimens for similar incident beam energies. It is to be noted that an increase in width of the O signal is usually observed at higher beam energies while probing the O concentration at larger depths, due to straggling of the beam. However, the peak area of the O signal remains constant for a homogeneous target. Presently we are unable to

explain the anomalous resonance peak widths in the Mn doped specimens.

Figure 3 shows the microstructure of undoped and 0.3–0.75 at.% Sb doped discs of type A. Exaggerated grain growth is observed in the undoped specimen with the grains being as large as 300 μm. However, the grain size decreases on doping, varying inversely with the concentration of dopants. The specimen doped with 0.3 at.% Sb consists of about 40 μm sized grain while the average grain size in the 0.5 at.% Sb doped sample is about 20 μm. The microstructure of the 0.75 at.% doped specimen consists of equisized uniform grains with an average grain size of about 2 μm. The microstructure of fractured surfaces of the sample shown in Fig. 3e further illustrates this feature. In the case of acceptor-doped specimens, the grains were 20–50 μm remaining large even for 1.0 at.% doping. The microstructures of 1.0 at.% Mn and Cu, and 0.5 at.% Zn doped discs of type A are shown in Fig. 4. On the other hand the average grain size of the undoped as well as donor and acceptor doped discs-B is <2 μm. The results are summarized in Table 2.

The growth of larger grains in Ti-rich specimens is ascribed to liquid phase sintering resulting from the existence of an eutectic reaction at 1,320 °C in the $BaTiO_3$–TiO_2 system. On the other hand Ba rich specimens have fine-grained microstructure, as in the absence of a liquid phase former the densification proceeds only through solid-state diffusion. The surface enhancement of Ti and Ba in specimens with large and fine-grained microstructure, respectively, reflects the above mechanism. The present study also indicates that donors inhibit grain growth while the acceptors do not have similar pronounced effects. Therefore the fine-grained microstructure of the undoped disc-B can be attributed to the presence of high concentration of donor impurities. To ascertain this undoped discs-A and B were analysed by inductively coupled plasma optical emission spectroscopy (ICP-OES). The concentration of donor impurities, as is usually the case, was found to be less. It was also observed that the content of impurities, except Sr, in specimens prepared by either method was identical. The concentration of Sr in the undoped disc-B was about 1,000 ppm whereas it was about 10 ppm in disc-A. Therefore it can be inferred that the fine microstructure of undoped disc-B is not due to donor impurities. The other factors contributing to such microstructure is the morphology of the powder as the gel-to-crystallite method produces nanosized particles and the presence of residual OH^-

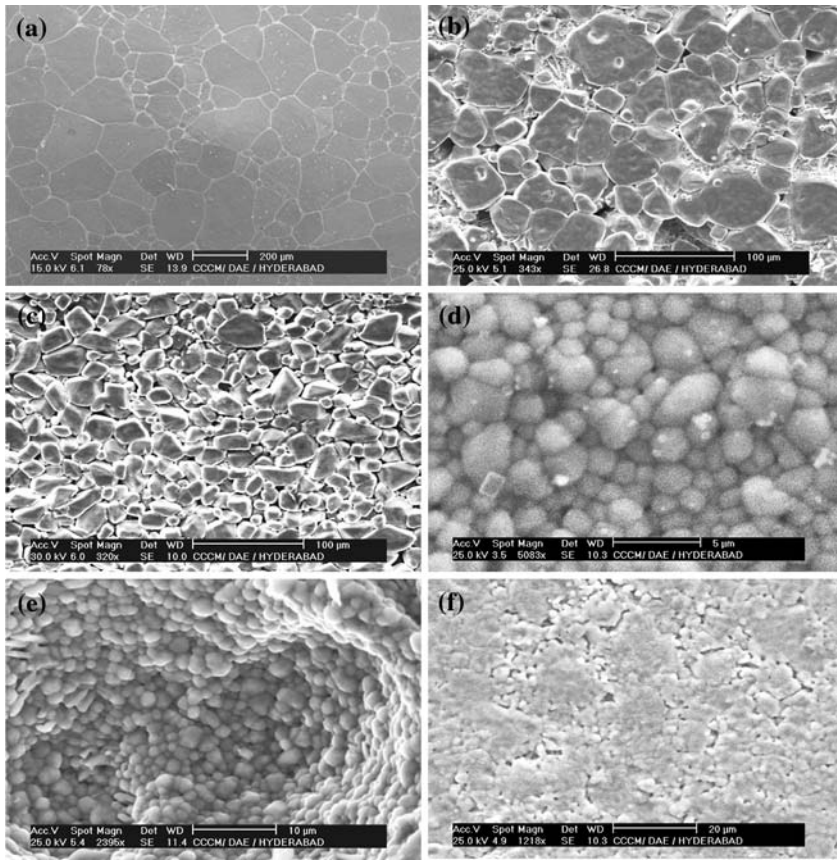

Fig. 3 SEM micrographs of (**a**) undoped, (**b**) 0.3 at.%, (**c**) 0.5 at.%, (**d**) 0.75 at.% Sb doped barium titanate discs derived by oxalate precursor method. The micrograph of the fractured surface of 0.75 at.% Sb doped specimen is shown in (**e**) while (**f**) shows the 0.3 at.% Sb doped specimen derived by gel to crystallite conversion

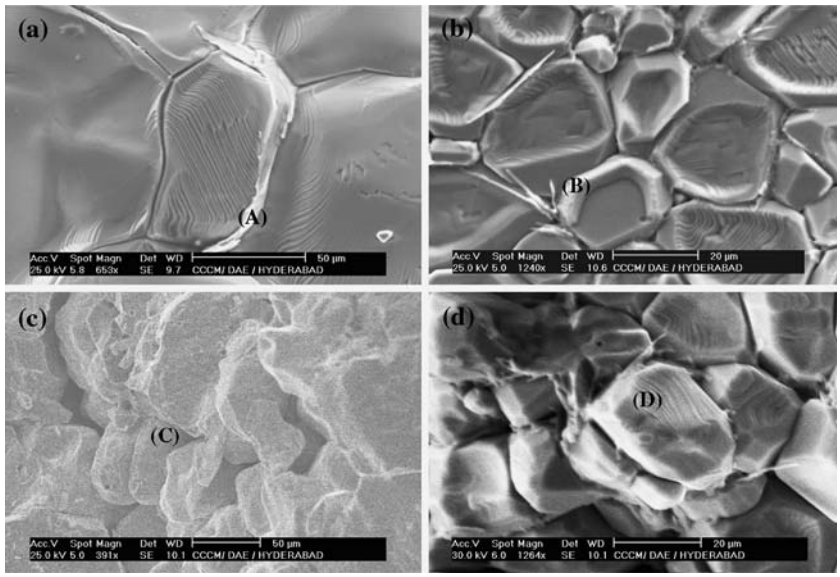

Fig. 4 SEM micrographs of (**a**) 1.0 at.% Cu and (**b**) 0.5 at.% Zn doped barium titanate specimens. The images of fractured surfaces of 1.0 at.% Mn and 0.5 at.% Zn doped specimens are shown in (**c**) and (**d**), respectively

Table 2 Grain size in undoped and doped barium titanate ceramics

Specimen	Range of grain size (μm)	Average grain size (μm)
Undoped (oxalate precursor)	42–308	135
0.3 at.% Sb doped (oxalate precursor)	9–78	40
0.5 at.% Sb doped (oxalate precursor)	5–42	20
0.75 at.% Sb doped (oxalate precursor)	1–5	2
0.5 at.% Zn doped (oxalate precursor)	50–87	50
1.0 at.% Zn doped (oxalate precursor)	7–36	20
1.0 at.% Cu doped (oxalate precursor)	50–100	55
Undoped (gel to crystallite)	1–4	1.5

groups that hinder the grain growth [11]. The higher concentration of Sr in discs-B further corroborates enrichment of Ba in specimens prepared by gel-to-conversion route.

Microarea elemental analysis by EDS to investigate the segregation of acceptors and donors at the grain boundaries of the ceramics proved challenging due to rather poor sensitivity of the technique in comparison to methods such as SIMS and also due to matrix effects as a result of smaller contents of the dopants. The grain boundaries chosen for profiling were oriented towards the EDS detector that facilitated the detection of X-rays without any significant absorption. The presence (or absence) of Mn, Cu and Zn was ascertained by detecting their respective K_α X-rays of energies 5.9, 8.05 and 8.6 keV. The measurements indicated segregation of dopants at the grain boundaries. Figure 5 shows the X-ray spectra recorded for 1.0 at.% Mn and Cu, and 0.5 at.% Zn doped specimens from the locations indicated at grain boundaries in Fig. 4. The presence of Zn was also observed, albeit in lesser amount, at the fractured surface shown in Fig. 4d, which is of intergranular nature. It was also observed that Si, an isovalent impurity, and other background acceptor impurities segregated along with the dopant at the grain boundaries and interfacial regions. In the case of donor doped ceramics, Sb-L X-rays (3.6 keV) could not be detected during the examination of several grains and grain boundaries. The detection of Sb-L X-rays is difficult on two accounts, (a) high background in the relevant energy region due to Ba and Ti X-rays and (b) smaller concentration of Sb. In fact the first factor is dominant that the signals cannot be detected unless severe segregation occurs. On the other hand considerable reduction in grain sizes on increasing the concentration of dopants makes the microanalysis along the grain boundaries even more difficult. It is be noted that acceptors could be detected rather easily due to larger grain sizes and low background in high energy regions (>5.5 keV).

The segregation of Mn and Cu at the grain boundaries was accompanied with enrichment of Ti. It was observed by comparing the intensity ratio of Ba-L_α and Ti K_α X-rays at grain interiors and locations of segregation in the grain boundaries. As mentioned earlier, in the EDS analysis of barium titanate a quantitative evaluation of Ba/Ti ratio is difficult due to overlap of Ba-L_α and Ti-K_α as well as Ba-L_β and Ti-K_β X-rays. However Ba-L_γ does not suffer from any

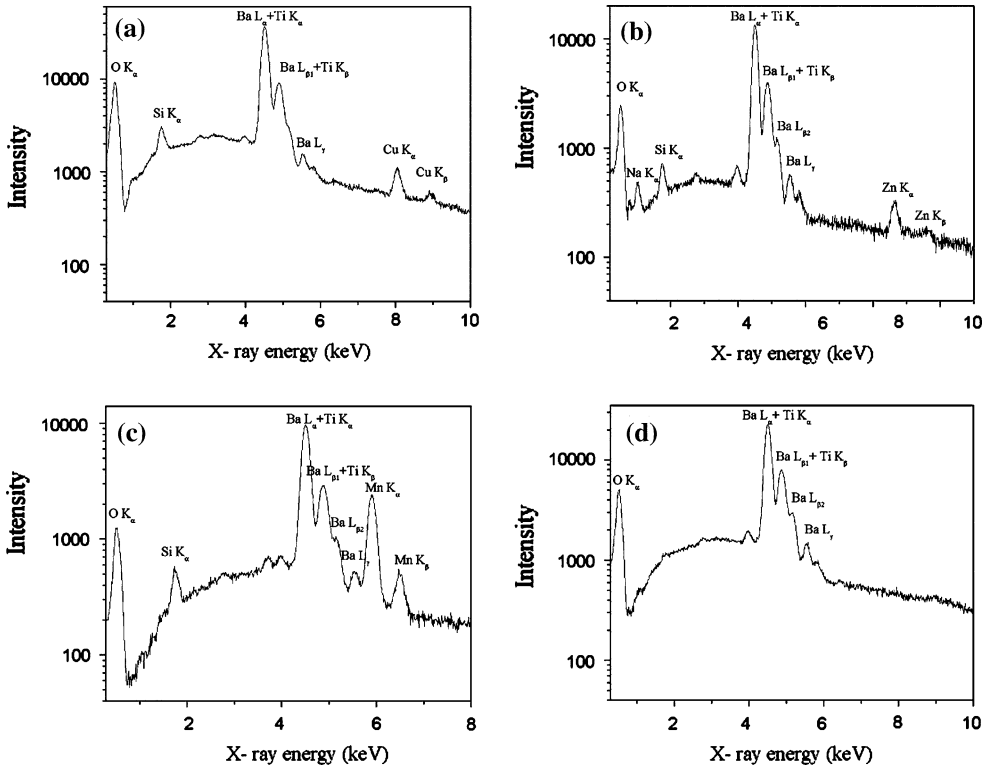

Fig. 5 X-ray spectra at the grain boundaries of (**a**) 1.0 at.% Cu, (**b**) 0.5 at.% Zn, (**c**) 1 at.% Mn doped barium titanate showing segregation of Cu, Zn and Mn, respectively. The X-ray spectra of a grain interior in 1 at.% doped Cu is shown in (**d**)

interference. Therefore, the contribution of Ba-L_α in the sum peak of Ba-L_α and Ti-K_α X-rays at 4.5 keV and in turn, the ratio of their intensities $(I_{K_\alpha})_{Ti}/(I_{L_\alpha})_{Ba}$ were obtained by taking the branching ratio and intensity of Ba-L_γ X-rays into consideration. The values of $(I_{K_\alpha})_{Ti}/(I_{L_\alpha})_{Ba}$, shown in Fig. 6, ranged from 3.5 to 4.4 at the grain boundaries and 1.2–2.0 in the grain interiors, demonstrating the enrichment of Ti at the locations of segregation of Mn and Cu. It might have also led to the formation of secondary titanate phases involving the acceptors, which escaped detection by XRD due to their less net concentration. However, this value remained the same (1.5–2.0) throughout the Zn doped specimen. Interestingly, Chiang and Takagi using scanning transmission electron microscopy (STEM) also observed Ti and acceptor enrichment at the grain boundaries [18].

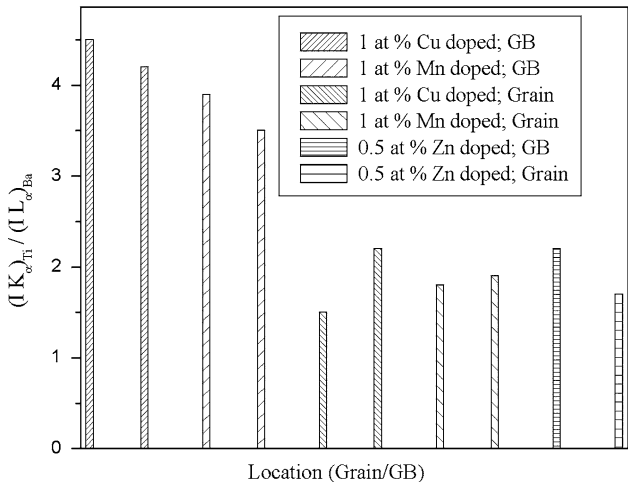

Fig. 6 Intensity ratio of Ti K_α and Ba L_α X-rays at grain boundaries and grains in the Mn, Cu and Zn doped barium titanate specimens. The measurements at grain boundaries are made at the locations of segregation

The peak at about 120 °C in the dielectric constant-temperature plot for a specimen with higher Ti content, for example 0.75 at.% Sb doped disc-A, depicted in Fig. 1a corresponds to the transition in the crystal structure of barium titanate from tetragonal to cubic phase. This transition is sharp and is accompanied with a change in dielectric constant according to the Curie–Weiss law, which is typical of normal ferroelectrics. In contrast, dielectric constant–temperature plot shown in Fig. 1b for 0.3 at.% Sb doped disc-B having relatively higher Ba content, has diffuse transition characteristics with transition peaks suppressed considerably. These results suggest that the microstructure and the electrical properties are intimately related to the relative content of Ba and Ti at the surface. On the other hand, the electrical characteristics of barium titanate are known to depend on the oxygen concentration as well. This requires estimation

of oxygen with greater accuracy and precision. In this regard, deuteron induced gamma ray emission (DIGME), employed for high precision determination of oxygen in high T_c superconductors would be an interesting ion beam technique [19].

Conclusions

Backscattering spectrometry studies indicate that (a) the cationic compositions of barium titanate discs in surface and near surface regions are different from the nominal stoichiometry and (b) Mn doped ceramics, exhibiting hexagonal phase, is deficient in oxygen. The specimens derived by oxalate precursor method exhibit coarse to fine grained microstructure depending on the nature and extent of doping while those prepared by gel to crystalline method are always fine grained. Microarea analysis by EDS showed segregation of acceptors such as Mn, Cu and Zn in the grain boundaries and is accompanied by Ti enrichment.

Acknowledgement The first two authors thank Dr T. Mukherjee, Director, Chemistry Group, BARC and Dr J. Arunachalam, Head, NCCCM, Hyderabad, for fruitful discussions and constant encouragement.

References

1. Haertling GH (1999) J Am Cer Soc 82:797
2. Phule PP, Risbud HS (1990) J Mater Sci 25:1169
3. Daniels J, Härdtl KH, Wernicke R (1978/1979) Philips Tech Rev 38:73
4. Lines ME, Glass AM (1979) Principles and applications of ferroelectric and related materials. Clarendon Press, Oxford
5. Moulson AJ, Herbert JM (1990) Electroceramics. Chapman and Hall, London UK, p 69
6. Kumar S, Raju VS, Kutty TRN (2003) Appl Surf Sci 206:250
7. Desu SB, Payne DA (1990) J Am Ceram Soc 73:3398
8. Horvath G, Gerbliner J, Mexiner H, Giber J (1996) Sens Actuators B 32:93
9. Rauhala E, Keinonen J, Jarvinen R (1988) Appl Phys Lett 52:1520
10. Murthy HSG, Subba Rao M, Kutty TRN (1975) J Inorg Nucl Chem 37:891
11. Kutty TRN, Padmini P (1995) Mat Chem Phys 39:200
12. Chu WK (1978) Backscattering spectrometry. Academic Press, NY, p 133
13. Leavitt JA, McIntyre LC Jr, Ashbaugh MD, Oder JG, Lin Z, Dezfouly-Arjomandy B (1990) Nucl Instr Meth B 44:260
14. Mayer M (1997) SIMNRA User's Guide, Report IPP 9/113. Max-Planck-Institut für Plasmaphysik, Garching, Germany
15. Kutty TRN, Devi LG, Murugraj P (1986) Mater Res Bull 22:1093
16. Gery IE, Li C, Cranswick LMD, Roth RS, Vanderah TA (1998) J Solid State Chem 135:312
17. Jia CL, Urban K (2004) Science 303:2001
18. Chiang YM, Takagi T (1990) J Am Ceram Soc 73:3278
19. Vickridge I, Tallon J, Preslad M (1994) Nucl Instr Meth B 85:95